Proceeding of the 2004 American Control Conference
Boston, Massachusetts June 30 - July 2, 2004

Control of Dynamics-Coupling Effects in Piezo-Actuator for High-Speed AFM Operation†

Szuchi Tien Qingze Zou S. Devasia‡
Mechanical Engineering Department, Box 352600, Univ. of Washington, Seattle, Washington 98195

***Abstract*— This article addresses the compensation for the dynamics-coupling effects in piezo-actuators used for positioning in atomic force microscopes (AFMs). Piezo-actuators are used to position the AFM probe (relative to the sample) both parallel to the sample surface (x-y-axes) and perpendicular to the sample surface (z-axis). During AFM operation, such as nanofabrication and imaging of soft biological samples, the probe-sample distance (in the z-axis) needs to be precisely controlled to maintain the probe-sample interaction at a desired value; otherwise, large variation of the probe-sample distance will result in distortions of the fabricated parts (in nanofabrication) and can cause sample damage (in imaging soft biological samples). In this article, we show that dynamics-coupling from the x-y-axes (the scanning axes) to the z-axis, referred to as x-to-z dynamics-coupling, can generate significant variations in the probe-sample distance when operating AFM at high speed, i.e., when the sample is scanned at high speed. We present an inversion-based approach to compensate for these dynamics-coupling effects. Additionally, for applications where the x-y-axes movement is repetitive (as in AFM scanning operations), an iterative approach is proposed to further reduce the coupling-caused positioning errors. Convergence of the iterative approach is investigated and experimental results show that the coupling-caused errors can be reduced to the noise level using the proposed approach. Thus, the main contribution of this article is the development of an approach to substantially reduce the coupling-caused positioning errors and thereby, enable high-speed high-precision positioning of piezoscanners used in AFMs.**

I. INTRODUCTION

This article addresses a critical dynamics-coupling problem that arises during high-speed nano-precision positioning using piezo tube-scanners (piezoscanners). It is noted that piezoscanners are extensively used in scanning-probe microscopes such as the atomic force microscope(AFM). For example, in AFM applications, the piezoscanner is used to position a probe over a sample, both parallel to the sample surface (x-y-axes) and perpendicular to the sample surface (z-axis). As the probe is scanned across the sample (in the x-y-axes), the probe-sample interactions (such as probe-sample forces) can be used (a) to investigate nano-scale surface properties in imaging applications (e.g., [1], [2]) and (b) to modify the surface properties in nano-fabrication applications (e.g., [3], [4]). During such nano-imaging and nano-fabrication operations, it is important to precisely control the probe-sample interactions because large variations in probe-sample interactions result in the distortions of the fabricated parts in nanofabrication and cause sample damage when imaging soft biological samples. Since the probe-sample interaction depends on the distance between the probe and the sample (referred to as the probe-sample distance) [4], it is important to precisely control the z-axis position during high-speed AFM operations. However, the x-to-z dynamics-coupling, that is the input of the scanning movement in the horizontal x-y-axes excites the dynamics of the piezo actuator in the vertical z-axis and generates the z-axis displacement and errors in the z-axis positioning (i.e., variation in the probe-sample distance), resulting in loss of precision control over the probe-sample interaction. These movement induced positioning errors become significant during high-speed operation of the AFM; thus, dynamics-coupling effects limit the throughput of AFMs. This article shows that the dynamics-coupling effects can be effectively modeled and compensated-for by using an inversion-based approach which reduces the error in the z-axis positioning. Additionally, for applications where the x-y-axes movement is repetitive (as in AFM scanning operations), an iterative inversion-based approach is proposed to further reduce the coupling-caused positioning errors. Convergence of the iterative approach is investigated and experimental results show that the coupling-caused errors can be reduced to the noise level with the proposed approach. Thus, the main contribution of this article is the development of an approach to substantially reduce coupling-caused errors and thereby, enable high-speed high-precision positioning with piezoscanners used in AFMs.

Compensating for the coupling-caused positioning error in the probe-sample distance (i.e., z-axis) is important in AFM applications such as nanofabrication (to avoid distortion of fabricated parts) and imaging of soft biological samples (to avoid sample damage and tip contamination). For example, nano-scale parts can be fabricated by using the AFM probe as an electrode to induce local-oxidation [4] by applying a voltage between the AFM probe and the surface. Since the probe-sample distance has a dominant effect on the formation of the oxide, coupling-caused positioning errors lead to the distortions in the size and shape of the nanofabricated parts [4]. Similarly, precision control of the probe-sample distance is needed to maintain small probe-sample forces when imaging soft biological samples such as living cells with an AFM [5], [6]. It is noted that the probe-sample force depends on the probe-sample distance. Therefore, errors in the probe-sample distance can lead to large probe-sample forces which cause the AFM-probe to protrude into the soft biological sample, damage the sample and contaminate the tip. Therefore, there is a need to develop techniques that reduce the coupling-caused positioning errors in high-precision AFM applications such as nanofabrication and imaging of soft biological samples.

Accounting-for the coupling-caused positioning errors is critical to increase AFM's throughput because the effects of these positioning errors become significant as the operating speed is increased. In particular, the coupling-caused positioning error becomes large when the scan frequency (at which the probe is scanned over the sample surface) is increased and approaches the vibrational-resonant frequency of the piezoscanner. The resulting movement-induced vibrations in the scan axes cause errors in the probe-sample distance due to dynamics-coupling (e.g., see [7]). One approach to avoid the dynamics-coupling effect is to constrain the AFM operation to low speeds. However, high-speed operation of the AFM is necessary in applications such as nanofabrication and imaging of biological samples. For example, high-speed AFM imaging is needed to study the time evolution of fast biological processes such as the rapid dehydration and denaturation of colla-

† Work Funded by NIH Grant GM68103 and NSF CMS 0301787
‡ Email: devasia@u.washington.edu, Tel: 206 685 3401

gen and the movement of human cells [5], [6]. Lack of sufficiently high-speed AFM results in image distortions because the sample topography and properties can change significantly during the time needed to acquire an image. Similarly, it is important to increase the AFM-operating speed to increase the throughput of AFM-based nanofabrication. Therefore, reducing the coupling-caused positioning errors will enable the development of high-throughput AFMs.

Compensating for the dynamics-coupling-caused positioning error is challenging because AFM-systems tend to have low gain margins. For example, feedback based techniques, such as the standard Proportional-Integral-Derivative (PID) or Integral (I) controller [8], can be used to reduce piezo positioning errors such as dynamics coupling effects [7]. In general, high-gain feedback can lead to substantial reduction of the positioning errors. However, feedback techniques have had limited success in compensating for piezo-positioning errors because the low gain margin of the piezoscanner limits the maximum feedback gain in order to ensure the stability of the closed-loop system [9], [10]. Recent development of advanced feedback controllers has lead to substantial improvement in AFM probe positioning [11], [12], [13]; however, the overall performance of feedback controllers continues to be limited by the low-gain-margin of piezoscanners.

The low-gain-margin limitation of feedback controllers can be alleviated by augmenting the feedback controller with feedforward inputs [13], [14]. For example, in the inversion-based feedforward approach, the dynamics of the piezoscanner is modeled and then inverted to find an input that achieves precision positioning of the piezoscanner [15], [16]. It is noted that the addition of this inversion-based feedforward input can improve the tracking performance of any feedback controller — even in the presence of computational errors due to modeling uncertainties (the size of acceptable uncertainties has been quantified in Ref. [17]). Previous results show that the feedforward input can be used to account for positioning errors in the scan axes (e.g., [14]). This article shows that the feedforward approach can also be used to reduce the coupling-caused positioning errors in vertical z axis and thereby, to reduce the variations in the probe-sample distance. Additionally, we use an inversion-based iterative control technique to further reduce the coupling-caused errors in the probe-sample distance in applications where these errors are repetitive. For example, during AFM imaging, the piezoscanner is used to repetitively scan the AFM probe over the sample, back and forth, resulting in the *repetitive* coupling-caused positioning errors in the z-axis — we show that these repetitive coupling errors can be substantially reduced using an iterative control approach. In particular, we present a frequency domain interpretation for the convergence of an inversion-based iterative approach proposed in [18], [19] and use the analysis to design the iteration procedure. The inversion-based iterative feedforward approach was implemented on an example piezoscanner and experimental results are presented to show that the dynamic-coupling-caused positioning error can be significantly reduced, close to the noise level of the sensors, by using the proposed iterative control method.

The rest of the article is organized as follows. The coupling problem is formulated in Section 2. The inversion-based iterative control algorithm and the convergence analysis are presented in Section 3. The proposed control technique is applied to an example piezoscanner and experimental results are presented with discussions in Section 4. Our conclusions are in Section 5.

II. Dynamics-Coupling Effects in Piezoscanner

A. Modeling the Dynamics-Coupling Effect

The piezoscanner is used to spatially position and scan the AFM-probe relative to the sample surface. The piezoscanner enables positioning of the AFM probe both parallel (along the x and y-axis) and perpendicular (along the z-axis) to the sample surface. Coupling-caused positioning errors in the z-axis can arise due to the scanning movement in the x and y axes. However, the effect of y-axis movement on the z-axis position tends to be less significant because the scan frequency in the y-axis is substantially smaller than the scan frequency in the x-axis. Therefore, the most prominent movement-induced coupling vibration in AFM is caused in the z-axis due to the scanning movement in the x-direction. Although the inversion-based approach can be used to correct movement-induced vibrations from both x and y scan axes, we focus this article on the reduction of the x-axis coupling effects to illustrate the proposed approach. Therefore, the z-axis displacement of the piezoscanner $z(t)$ is modeled as the linear combination of the displacements due to the z-axis input $u_z(t)$ and the coupling effect from the x-axis input $u_x(t)$, i.e., the z-axis displacement can be written in the frequency domain as

$$\begin{aligned} z(j\omega) &= G_{zz}(j\omega)u_z(j\omega) + G_{zx}(j\omega)u_x(j\omega) \\ &\triangleq z_z(j\omega) + z_x(j\omega) \end{aligned} \quad (1)$$

where $z(j\omega),\ u_z(j\omega),\ u_x(j\omega)$ are the Fourier Transform of $z(t),\ u_z(t)$ and $u_x(t)$ respectively, $G_{zz}(j\omega) = z_z(j\omega)/u_z(j\omega)$ is the transfer function that describes the linear dynamics in the z-axis direction, and $G_{zx}(j\omega) = z_x(j\omega)/u_x(j\omega)$ is the transfer function that describes the x-to-z coupling dynamics.

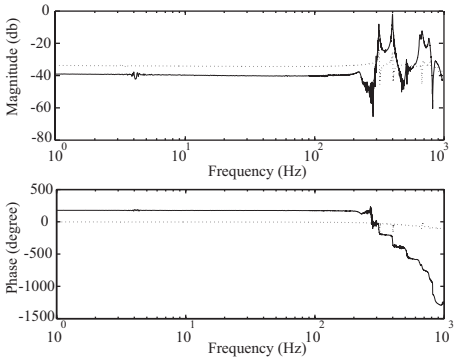

Fig. 1. Bode plots of the example piezoscanner: x-to-z coupling dynamics $G_{zx}(j\omega)$ (solid line) and the z-to-z dynamics $G_{zz}(j\omega)$ (dashed line)

Dynamics-Coupling Becomes Significant During High-Speed Scanning. The increase in x-to-z dynamics-coupling effect with scan frequency can be evaluated by comparing the relative magnitudes of the frequency responses of the x-to-z coupling dynamics $G_{zx}(j\omega)$ at different scan frequencies. The frequency responses ($G_{zx}(j\omega)\ and\ G_{zz}(j\omega)$), for the example piezoscanner studied in this article, are shown in Fig. 1. Note that the x-to-z dynamics-coupling effect is relatively small at small scan frequencies. For example, at $10Hz$, the magnitude of the x-to-z coupling dynamics $G_{zx}(j\omega)$ is $-39.7\ db$ which is about 52% of the magnitude $-34.1db$ of the z-to-z dynamics $G_{zz}(j\omega)$. However, as scan frequency increases, the magnitude of x-to-z coupling dynamics $G_{zx}(j\omega)$ becomes substantially larger than the z-to-z dynamics $G_{zz}(j\omega)$. For example, at

313 Hz (the first resonant peak in Fig. 1), the magnitude of coupling effect $G_{zx}(j\omega)$ is -8.5 db, which is 6.5 times larger than the magnitude -24.8 db of the z-to-z dynamics $G_{zz}(j\omega)$. The coupling effect has increased from -39.7 db to -8.5 db as the scan frequency is increased from $10Hz$ to $313Hz$; therefore, the x-to-z coupling effect becomes significant and should be compensated-for as the scan frequency is increased.

Dynamics-Coupling Can Cause Large Errors in the z-axis Displacement. The relatively large magnitude of the x-to-z dynamics-coupling effects is show in Figure 2, which presents the x-axis displacement and the corresponding coupling-caused z-axis displacement. For a 100Hz, 30 μm (peak-to-peak) scan in the x-axis (see upper plot in Fig. 2), the coupling-caused z-axis displacement is about 1 μm (bottom plot in Fig. 2). It is noted that the x-axis scan range of 30 μm is consistent with the scan range needed to image relatively-large biological sample such as living cells [1]. However, the 1 μm coupling-caused positioning errors in the z-axis is not acceptable in nano-positioning applications such as AFM imaging of soft biological samples that requires nanometer-range control of the probe-sample distance [5]. Therefore, the experimental data in Fig. 2 shows that the x-to-z dynamics coupling must be accounted-for to enable high-precision high-speed positioning with piezoscanners.

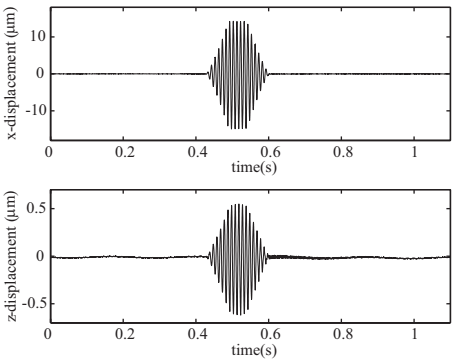

Fig. 2. Experimental Results: x-axis displacement with a scan range of 30 μm (upper plot) and the corresponding x-to-z coupling-caused positioning error in the z-axis of the piezoscanner.

B. Dynamics-Coupling Problem Formulation

An inversion-based feedforward/feedback approach is used to compensate for the x-to-z dynamics-coupling. The control scheme is shown in Fig. 3, where the z-axis control input $u_z(j\omega)$ is the combination of the feedback input $u_{fb}(j\omega)$ and the feedforward input $u_{ff}(j\omega)$,

$$u_z(j\omega) = u_{fb}(j\omega) + u_{ff}(j\omega) \tag{2}$$

From Eqs. (1,2) (and Fig. 3), the z-axis output $z(j\omega)$ can be re-written as

$$\begin{aligned} z(j\omega) &= G_{ff}(j\omega)u_{ff}(j\omega) + \hat{G}_{zx}(j\omega)u_x(j\omega) + G_{fb}(j\omega)z_d(j\omega) \\ &\triangleq z_{ff}(j\omega) + z_x(j\omega) + \hat{z}_d(j\omega) \end{aligned} \tag{3}$$

where $z_d(j\omega)$ is the desired z-axis position, $\hat{z}_d(j\omega)$ is the achieved z-position in the absence of the x-to-z dynamics-coupling, and

$$G_{fb}(j\omega) \triangleq G_{zz}(j\omega)G_c(j\omega)\mathsf{S}_z(j\omega) \tag{4}$$

$$G_{ff}(j\omega) \triangleq G_{zz}(j\omega)\mathsf{S}_z(j\omega) \tag{5}$$

$$\hat{G}_{zx}(j\omega) \triangleq G_{zx}(j\omega)\mathsf{S}_z(j\omega) \tag{6}$$

where $\mathsf{S}_z(j\omega)$ is the *sensitivity* of the closed-loop system,

$$\mathsf{S}_z(j\omega) \triangleq \frac{1}{1 + G_{zz}(j\omega)G_c(j\omega)}. \tag{7}$$

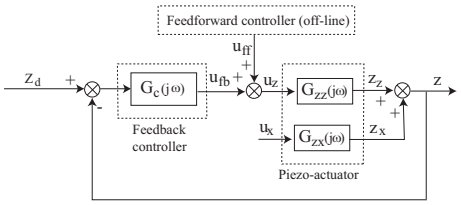

Fig. 3. The control scheme to compensate the x-to-z dynamics-coupling of the piezoscanner, where $G_{zz}(j\omega)$ and $G_{zx}(j\omega)$ are the transfer functions of the z-to-z dynamics and x-to-z dynamics, respectively

This article focuses on the development of the feedforward input $u_{ff}(t)$ to compensate for the x-to-z dynamics-coupling. This feedforward input can be implemented with any feedback controller G_c such as the more advanced feedback approaches presented in Refs. [10-12].

Dynamics-Coupling Compensation Problem For a given lateral x-axis input $u_x(j\omega)$ and a desired vertical z-axis trajectory, the dynamics-coupling compensation problem is to find the z-axis feedforward control input $u_{ff}(j\omega)$, such that the coupling-caused z-axis displacement can be removed when this control input $u_{ff}(j\omega)$ is applied, i.e.,

$$G_{ff}(j\omega)u_{ff}(j\omega) + \hat{G}_{zx}(j\omega)u_x(j\omega) = z_{ff}(j\omega) + z_x(j\omega) = 0 \tag{8}$$

III. Inversion-Based Dynamics-Coupling Compensation

In this section, we present an inversion-based approach to compensate for the x-to-z dynamics-coupling. First, the the feedforward input is obtained by inverting the dynamics of piezoscanner. Second, this initial inverse input is used as an initial condition for an iterative procedure which can be used in applications where the lateral x-axis operation is *repetitive*. Then, the convergence of the iterative approach is analyzed and used to select parameters of the iteration algorithm.

A. Inversion-based Feedforward Control

The inverse input to compensate for the x-to-z dynamics-coupling can be obtained by using Eq. (8) as

$$u_{ff,i}(j\omega) = -G_{ff}^{-1}(j\omega)\hat{G}_{zx}(j\omega)u_x(j\omega) \tag{9}$$

Exact cancelation of the coupling-caused z-axis displacement can be obtained, provided that there is no error in the dynamics models $G_{ff}(j\omega)$ and $\hat{G}_{zx}(j\omega)$. Even in the presence of modeling errors, this inversion-based feedforward method can reduce the coupling-caused z-axis displacement if the modeling error is small — as noted before, the acceptable modeling error for applying the inversion-based feedforward input has been quantified in [17].

B. Inversion-based Iterative Control

To account for modeling errors in the computation of the inverse input in Eq. (9), we present a frequency domain interpretation for the convergence of an inversion-based iterative approach proposed

in [18], [19] and use the analysis to design the iteration procedure. The iterative control law is given as

$$\begin{aligned} u_{ff,0}(j\omega) &= 0, && (10)\\ u_{ff,k}(j\omega) &= u_{ff,\ k-1}(j\omega) && (11)\\ &\quad +\rho G_{ff}^{-1}(j\omega)\left[z_{ff}(j\omega) - z_{ff,k-1}(j\omega)\right] \quad (k \geq 1) \end{aligned}$$

where $u_{ff,0}(j\omega)$ is the initial condition, $\rho \in \Re$ is the iteration coefficient used at each iteration, $z_{ff}(j\omega)$ is defined in Eq. (8), $u_{ff,k}(j\omega)$ is the Fourier Transform of the z-axis feedforward input at the k^{th} iteration, $u_{ff,k}(t)$, and $z_{ff,k}(j\omega)$ is the corresponding z-axis displacement.

Remark 1: During repetitive operations, $z_{ff}(j\omega) = -z_x(j\omega)$ can be obtained from experimental measurements when the x-axis input $u_x(j\omega)$ is applied alone.

Remark 2: The inverse feedforward input from Eq. (9) can be chosen as the initial inverse input $u_{ff,0}(j\omega)$ for the iteration process. Such choice of initial value of the iterative control input can reduce the number of iterations.

C. Convergence Analysis for the Iterative Control Law

In the following, the convergence of the iterative learning control law Eqs. (10, 11) is quantified in terms of the error in modeling the system's dynamics. Let the variation $\Delta G(j\omega)$ between the model of the system's dynamics $G_{ff}(j\omega)$ and the actual system's dynamics $G_{ff,o}(j\omega)$ be described by

$$\begin{aligned} \Delta G(j\omega) &= G_{ff}(j\omega)^{-1} G_{ff,0}(j\omega)\\ &= \frac{r_{ff,0}(\omega)\ e^{j\theta(\omega)}}{r_{ff}(\omega)e^{j\tilde{\theta}(\omega)}} = \Delta r(\omega) e^{j\Delta\theta(\omega)} \end{aligned} \quad (12)$$

where $\Delta r(\omega)$ represents the magnitude variation and $\Delta\theta(\omega) \in \Re$ represents the phase variation at frequency ω. The convergence of the iterative control law (Eq. (11)) is given by the following lemma.

Lemma 1: Let the actual system dynamics $G_{ff,o}(j\omega)$ and its model $G_{ff}(j\omega)$ be stable, and let ω be a frequency where both $G_{ff,o}(j\omega)$ and $G_{ff}(j\omega)$ do not have zeros at $\pm j\omega$ (i.e., $\Delta r(\omega) > 0$ in Eq. (12)). Then, the output converges to the desired-feedforward trajectory, i.e., $\lim_{k\to\infty} z_{ff,k}(j\omega) = z_{ff}(j\omega)$, by using the iterative control law (Eq. (11)), if and only if

1) The magnitude of phase variation is less than $\pi/2$, i.e., $|\triangle\theta(\omega)| < \pi/2$, at frequency ω;
2) The iteration coefficient ρ in Eq. (11) is chosen as

$$0 < \rho < \tfrac{2\cos(\Delta\theta(\omega))}{\Delta r(\omega)} \quad (13)$$

Proof: The iterative control law Eq. (11) can be re-written using Eq. (12) as

$$\begin{aligned} &u_{ff,k}(j\omega)\\ &= u_{ff,k-1}(j\omega) + \rho G_{ff}^{-1}(j\omega)\left[z_{ff}(j\omega) - z_{ff,k-1}(j\omega)\right]\\ &= u_{ff,k-1}(j\omega) + \rho G_{ff}^{-1}(j\omega) \times\\ &\quad \left[G_{ff,0}(j\omega)u_{ff}(j\omega) - G_{ff,0}(j\omega)u_{ff,k-1}(j\omega)\right]\\ &= u_{ff,k-1}(j\omega) + \rho\Delta G(j\omega)\left[u_{ff}(j\omega) - u_{ff,k-1}(j\omega)\right] \end{aligned} \quad (14)$$

Then, for any given $\omega \in \Re$, the difference between the feedforward input $u_k(j\omega)$ computed at k-th iteration and the desired input, $u_{ff}(j\omega)$ can be written using Eq. (14) as,

$$\begin{aligned} |u_{ff,k}(j\omega) - u_{ff}(j\omega)| &= |u_{ff,k-1}(j\omega) - u_{ff}(j\omega)\\ &\quad - \rho\Delta G(j\omega)\left[u_{ff,k-1}(j\omega) - u_{ff}(j\omega)\right]|\\ &= |u_{ff,k-1}(j\omega) - u_{ff}(j\omega)||1 - \rho\Delta G(j\omega)|\\ &= |u_{ff,k-1}(j\omega) - u_{ff}(j\omega)||1 - \rho\Delta r(\omega)e^{j\Delta\theta(\omega)}| \end{aligned} \quad (15)$$

Repeated application of Eq. (15) leads to

$$\begin{aligned} &|u_{ff,k}(j\omega) - u_{ff}(j\omega)|\\ &\quad = |1 - \rho\Delta r(\omega)e^{j\Delta\theta(\omega)}|^k |u_{ff,0}(j\omega) - u_{ff}(j\omega)| \end{aligned} \quad (16)$$

Therefore, the iterative control law converges, i.e.,

$$\lim_{k\to\infty} |u_{ff,k}(j\omega) - u_{ff}(j\omega)| = 0$$

if and only if the mapping coefficient $|1 - \rho\Delta r(\omega)e^{j\Delta\theta(\omega)}| < 1$, or equivalently,

$$\begin{aligned} |1 &- \rho\Delta r(\omega)e^{j\Delta\theta(\omega)}|^2\\ &= |1 - \rho\Delta r(\omega)[\cos(\Delta\theta(\omega)) + j\sin(\Delta\theta(\omega))]|^2\\ &= (1 - \rho\Delta r(\omega)\cos(\Delta\theta(\omega)))^2 + (\rho\Delta r(\omega)\sin(\Delta\theta(\omega)))^2\\ &= 1 - 2\rho\Delta r(\omega)\cos(\Delta\theta(\omega)) + \rho^2(\Delta r(\omega))^2 \ < \ 1 \end{aligned} \quad (17)$$

Eq. (17) can be simplified as

$$\rho\left(\rho\Delta r(\omega) - 2\cos(\Delta\theta(\omega))\right) \ < \ 0 \quad (18)$$

Since $\Delta r(\omega) > 0$, the Eq. (18) is satisfied if and only if 1) $\cos(\triangle\theta(\omega)) \neq 0$, i.e., $\triangle\theta(\omega) \neq \pi/2$ and its multiples; 2) the iterative coefficient ρ is choosen as

$$\begin{aligned} 0 < \rho < \tfrac{2\cos(\Delta\theta(\omega))}{\Delta r(\omega)}, &\quad \text{for } \cos(\Delta\theta(\omega)) > 0\\ \tfrac{2\cos(\Delta\theta(\omega))}{\Delta r(\omega)} < \rho < 0, &\quad \text{for } \cos(\Delta\theta(\omega)) < 0 \end{aligned} \quad (19)$$

However, since the variation of system dynamics is continuous, the phase variation with a magnitude larger than $\pi/2$ will result in the sign-flip of the function $\cos(\triangle\theta(\omega))$ (i.e., from $\cos(\triangle\theta(\omega)) > 0$ to $\cos(\triangle\theta(\omega)) < 0$, or vice versa) during the iteration process. Note that, this sign-flip is not known a priori because it can be caused by unknown factors such as disturbances. Therefore, it is not realistic to change ρ to accommodate such sign-flip during the iteration process. This completes the proof of Lemma 1. ■

Lemma 2: Let S_ω be set of frequencies where the modeling error satisfies the following

$$S_\omega \ \triangleq \ \{\omega \mid 0 < \Delta r(\omega) \text{ and } |\Delta\theta(\omega)| \leq \Delta\theta_{max} < \pi/2\}$$

then the iterative control law converges if the iteration coefficient $\rho(\omega)$ is chosen as

$$\begin{aligned} 0 < \rho(\omega) < \rho_{max}, &\quad \text{for } \omega \in S_\omega\\ \rho(\omega) = 0, &\quad \text{otherwise} \end{aligned} \quad (20)$$

where

$$\rho_{max} = \inf_{\omega\in S_\omega} \ \frac{2\cos(\Delta\theta(\omega))}{\Delta r(\omega)}.$$

Proof: The convergence of the iteration for frequency ω in the set S_ω follows from Lemma 1; and the iteration converges in the first step if $\rho(\omega) = 0$. ■

IV. Experimental Example: Piezoscanner

The proposed inversion-based approach to compensate for the x-to-z dynamics-coupling is applied to an example piezoscanner and experimental results are presented.

A. Experiment Set Up and Modeling

Experiment Set Up The piezoscanner studied in the experiment is shown in Fig. 4. The displacements at the end of the piezoscanner, in the x-axis and z-axis direction, are measured by inductive sensors. The feedback controller used to control the z-axis is a proportion-integral (PI) controller given by $G_c(s) = K_p + K_I/(s + a)$, where the controller parameters were tuned experimentally to reduce overshoot and rise time ($K_p = 10$,

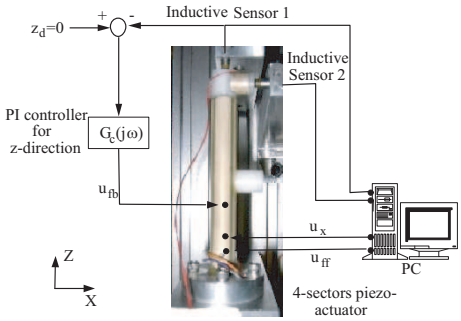

Fig. 4. The Schematic diagram of the experiment setup

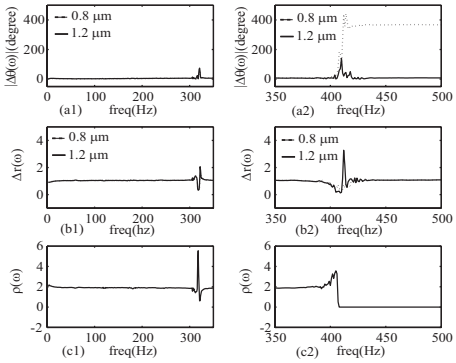

Fig. 5. The phase difference (plots (a1) and (a2)) and the magntiude difference (plots (b1) and (b2)) between the dynamics obtained at fixed output range of $0.8\ \mu m$ (dotted line), $1.2\ \mu m$ (solid line) and the dynamics obtained at output range of $0.2\ \mu m$. Plots (c1) and (c2) show the upper bound of $\rho(\omega)$ computed according to Eq. (13) for $\omega \in S_\omega$ and $\rho(\omega) = 0$ otherwise (see Lemma 2).

$K_I = 3393$, and $a = 10$).

Modeling the Dynamics We obtained the model of the x-to-z coupling dynamics, $\hat{G}_{zx}(j\omega)$, and the z-axis dynamics, $G_{ff}(j\omega)$ experimentally by using a digital signal analyzer (DSA). To reduce the range-dependent hysteresis effects, the linear models $\hat{G}_{zx}(j\omega)$ and $G_{ff}(j\omega)$ were obtained by fixing the output-displacement range at a low value of $0.2\ \mu m$, which is about 5% of the available displacement range in the z-axis. In addition, to quantify the magnitude and phase variation due to range-dependent effects, we obtained the z-axis dynamics model $G_{ff}(j\omega)$ at different displacement ranges. For example, the phase and magnitude variations for output ranges of $0.8\ \mu m$ and $1.2\ \mu m$ are shown in Fig. 5; these are used to estimate the phase and magnitude variations ($\Delta\theta(\omega)$ and $\Delta r(\omega)$) needed to design the iterative control law (see Lemma 2).

B. Implementation and Results

Coupling Effect: Experiment Results The x-to-z dynamics coupling caused displacement in the z-axis of the piezoscanner is shown in Fig. 6(a) when no z-axis control input is used to compensate for the coupling error. It is noted that the set point for the desired z-axis displacement was chosen to be zero for all the experiments. Next, the reduction of the coupling effects with the use of feedback is shown in Fig. 6(b); and the reduction of the coupling-caused errors with the addition of the inverse feedforward $u_{ff}(t)$ is shown in Fig. 6(c) (with the PI controller on).

Implementation of the Inversion-based iterative control Next we further reduced the coupling-caused z-axis errors by using the proposed iterative control law. We begin by quantifying the iteration coefficient $\rho(\omega)$ for frequency $\omega \in [0,\ 500]\ Hz$ (see Fig. 5). Note that plot (a1) shows that the phase variation $\Delta\theta(\omega)$ in the frequency range $[0,\ 350]\ Hz$ is less than $\pi/2$, i.e., $\cos(\Delta\theta(\omega)) > 0$ for $\omega \in [0,\ 350]\ Hz$; therefore, the maximum-value ρ_{max} of the iteration coefficient $\rho(\omega)$ can be computed from Lemma 2. This maximum value of ρ_{max} was 0.6 in the frequency range $[0,\ 350]\ Hz$; a smaller value $\rho(\omega) = 0.3$ was chosen as the iteration constant in the frequency range $\omega \in [0,\ 350]\ Hz$ for our experiment. On the other hand, plot (a2) shows that the phase variation becomes larger than $\pi/2$ after frequency around $410\ Hz$; therefore, $\rho(\omega)$ should be chosen as zero at those frequencies. To account for possible errors in quantifying the phase and magnitude variations, we set $\rho(\omega) = 0$ for frequency $\omega \in [350,\ 500]\ Hz$. This iteration coefficient $\rho(\omega)$ is used to implement the inversion-based iterative control law Eqs. (10, 11). The inverse feedforward input $u_{ff}(j\omega)$ given by Eq. (9) is applied as the input at the initial iteration (k=0), i.e., $u_{ff,0}(j\omega) = u_{ff,i}(j\omega)$.

Results with the Inversion-based iterative control The coupling-caused z-axis displacement is shown in Fig. 7(a) (when the inverse feedforward input $u_{ff}(t)$ is applied), the results for 4^{th} iteration and 7^{th} iteration are shown in Fig. 7, plots (b) and (c) respectively. To quantify the reduction of the coupling-caused z-axis displacement, the root-mean-square (RMS) error, e_{rms}, and maximum peak-to-peak error, e_{max}, are tabulated in Table I, where

$$\begin{aligned} e_{rms} &= \sqrt{[\int_0^{1.1} (z(t) - \bar{z})^2 dt]/1.1} \\ e_{max} &= |\max_{t\in[0,\ 1.1]} z(t) - \min_{t\in[0,\ 1.1]} z(t)| \end{aligned} \qquad (21)$$

$\bar{z}$ denotes the average value of z(t) and $[0,\ 1.1]$ is the time window during which the input were applied (and outputs were measured).

C. Discussion

Note that the experimental results show that significant coupling-caused displacement was generated in the z-axis (see Fig. 6(a)) due to the scanning movement in the lateral x-axis. By applying the inversion-based feedforward input, this coupling-caused z-axis displacement was dramatically reduced (see Fig. 6(c)). As shown in Table I, the RMS error e_{rms} and the maximum peak-to-peak error e_{max} are reduced from $0.1112\ \mu m$ and $1.1696\ \mu m$ to $0.0091\ \mu m$ and $0.1225\ \mu m$ respectively — reductions of 92% and 90% respectively. The inversion-based iterative control can be used to further eliminate the coupling-caused errors in the z-axis displacement. For example, the maximum error e_{max} due to coupling at 7^{th} iteration (see Table I) is comparable with the noise level of the signal. Therefore, by applying the inversion-based iterative control, we substantially reduced the coupling-caused z-axis displacement errors in piezoscanner during high-speed positioning— from micron range to the tens of nanometer range (which is the resolution of the inductive sensor). Further reduction is possible by using sensors with higher resolution such as the optical sensors used in AFMs. Therefore, the proposed inversion-based iterative control method can be used to enable high-speed high-precision AFM applications such as imaging of soft biological samples and nanofabrication.

V. Conclusions

This article showed that an inversion-based feedforward control can be used to compensate for the x-to-z dynamics-coupling errors

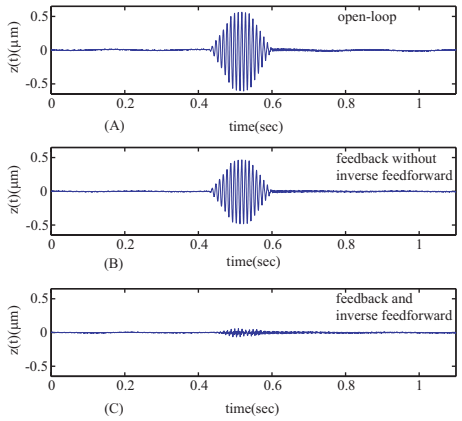

Fig. 6. The coupling-caused z-axis displacement without any control (plot (a)), with feedback PI-controller alone (plot (b)), and with the feedback PI-controller plus inversion-based feedforward input (plot (c)).

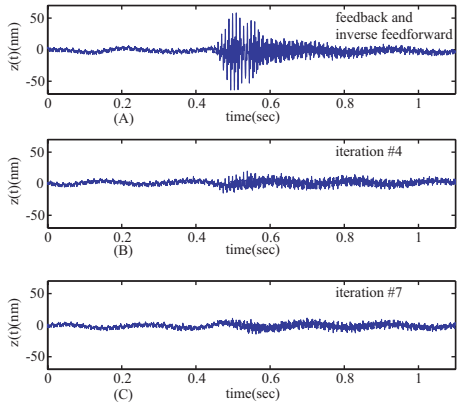

Fig. 7. The coupling-caused z-axis displacement by using the inversion-based feedforward input(plot (a)), at 4^{th} iteration (plot (b)) and at 7^{th} iteration (plot (c))(feedback controller is on in all cases).

TABLE I

z-AXIS DISPLACEMENT UNDER DIFFERENT CONTROL CONDITIONS.

Item	ρ	$e_{max}(\mu$m)	$e_{rms}(\mu$m)
No control	N/A	1.1696	0.1112
Feedback Only	N/A	0.9519	0.0917
Inversion	N/A	0.1225	0.0091
1^{st} Iter.	0.3	0.0886	0.0074
2^{nd} Iter.	0.3	0.0581	0.0052
3^{rd} Iter.	0.3	0.0398	0.0043
4^{th} Iter.	0.3	0.0350	0.0044
5^{th} Iter.	0.3	0.0288	0.0038
6^{th} Iter.	0.3	0.0274	0.0039
7^{th} Iter.	0.3	0.0257	0.0038
Noise Level	N/A	0.0108	0.0018

in piezoscanners during high-speed positioning. Additionally, an inversion-based iterative approach was used to further reduce effects of unmodeled dynamics. Convergence of the iterative approach was investigated and used to design the parameters of the iteration algorithm. Experimental results were presented to demonstrate (a) the presence of significant x-to-z coupling effects; and (b) substantial reduction of such coupling caused positioning errors (to the noise level) by using the proposed inversion-based iterative-feedforward approach.

REFERENCES

[1] C. Rotsch, F. Braet, E. Wisse, and M. Radmacher. Afm imaging and elasticity measurements on living rat liver macrophages. *Cell Biology International*, 21(11):685–696, 1997.

[2] S. Sundararajan and B. Bhushan. Development of afm-based techniques to measure mechanical properties of nanoscale structures. *Sensors and Actuators A*, 101:338–351, 2002.

[3] Chul Huh and Seong-Ju Park. Atomic force microscope tip-induced anodization of titanium film for nanofabrication of oxide patterns. *J. Vac. Sci. Technol. B*, 18(1):55–59, 2000.

[4] Emmanuel Dubois and Jean-Luc Bubendorff. Kinetics of scanned probe oxidation: Space-charge limited growth. *Journal of Applied Physics*, 87(11):8148–8154, 2000.

[5] C. Le Grimellec, E. Lesniewska, M.-C. Giocondi, E. Finot, V. Vie, and Goudonnet J.-P. Imaging of the surface of living cells by low-force contact-mode atomic force microscopy. *Biophysical Journal*, 75:695–703, Aug. 1998.

[6] F. El Feninat, T.H. Ellis, E. Sacher, and I. Stangel. A tapping mode afm study of collapse and denaturation in dentinal collagen. *Dental Materials*, 17:284–288, 2001.

[7] Osamah M. El Rifai and Kamal Youcef-Toumi. Coupling in piezoelectric tube scanners used in scanning probe microscopes. *Proceedings of the American Control Conference*, pages 3251–3255, 2001.

[8] Osamah M. El Rifai and Kamal Youcef-Toumi. Design and control of atomic force microscopes. *Proceedings of the American Control Conference*, pages 3714–3719, 2003.

[9] R. C. Barrett and C. F. Quate. Optical scan-correction system applied to atomatic force micropscopy. *Review of Scientific Instruments*, 62:1393–1399, 1991.

[10] J. A. Main and E. Garcia. Piezoelectric stack actuators and control system design: Strategies and pitfalls. *Journal of Guidance, Control, and Dynamics*, 20(3):479–485, May-June 1997.

[11] G. Schitter, A. Stemmer, and F. Allgöwer. Robust 2dof-control of a piezoelectric tube scanner for high speed atomic force microscopy. *Proceedings of the American Control Conference*, pages 3720–3725, 2003.

[12] S. Salapaka, A. Sebastian, J. P. Cleveland, and M. V. Salapaka. High bandwidth nano-positioner: A robust control approach. *Review of Scientific Instruments*, 73(9):3232–3241, Sept., 2002.

[13] Meng-Shiun Tsai and Jin-Shin Chen. Robust tracking control of a piezoacuator using a new approximate hysteresis model. *ASME Journal of Dynamics Systems, Measurement and Control*, 125:96–102, March 2003.

[14] Zou Q., Leang K. K., Sadoun E., Reed M. J., and Devasia S. Control issues in high-speed afm for biological applications: Collagen imaging example. *Special Issue on "Advances in Nano-technology Control", Asian Journal Control*, 2003. accepted with revision.

[15] D. Croft, G. Shedd, and S. Devasia. Creep, hysteresis, and vibration compensation for piezoactuators: Atomic force microscopy application. *ASME Journal of Dynamic Systems, Measurement and Control*, 123(35):35–43, March, 2001.

[16] H. Perez, Q. Zou, and S. Devasia. Design and control of optimal feedforward trajectories for scanners: Stm example. *Proceedings of the American Control Conference*, 3:2305–2312, 2002.

[17] S. Devasia. Should model-based inverse input be used as feedforward under plant uncertainty? *IEEE Trans. on Automatic Control*, 47(11):1865–1871, Nov. 2002.

[18] J. Ghosh and B Paden. Nonlinear repetitive control. *IEEE Trans. on Automatic Control*, 45(5):949–954, May 2000.

[19] Xuezhen Wang and Degang Chen. Robust inversion-based learning control for nonminimum phase system. *IEEE International Conference on System, Man, and Cybernetics*, 3, Oct. 2002.